Geomechanics and Engineering, *Vol. 14, No. 6 (2018) 601-614*
DOI: https://doi.org/10.12989/gae.2018.14.6.601

Behavior of integral abutment bridge with partially protruded piles

Min-Cheol Park[1a] and Moon S. Nam[*2]

[1]Department of Civil Engineering, Kumoh National Institute of Technology, 208 Global-gwan, 61, Daehak-ro, Gumi-si, Gyeongsangbuk-do, Republic of Korea
[2]Structure Research Division, Research Institute of Korea Expressway Corporation, 208-96, Dongbu-daero 922beon-gil, Dongtan-myeon, Hwaseong-si, Gyeonggi-do, Republic of Korea

(Received January 4, 2017, Revised December 28, 2017, Accepted January 1, 2018)

Abstract. This study presents structural and parametric analyses on the behavior of an integrated and pile-bent abutment with mechanically stabilized earth wall (IPM) bridge. The IPM bridge is an integral abutment bridge (IAB) with partially protruded piles, which excludes earth pressure by means of a mechanically stabilized earth wall developed by the authors. The results of the analysis indicate that the IPM bridge, as any other IAB, is influenced to a large extent by temperature and time-dependent loads. When these loads are applied, the stress on a pile in the IPM bridge decreases as the displacement of the pile top increases, because the piles protrude from the ground surface and no soil reaction is generated on the protruded pile. Because the length of an IAB is restricted by the forces acting on its piles, the IPM bridge is an effective alternative to extend its length.

Keywords: IPM bridge; structural analysis; protruded pile; pile behavior; seasonal behavior

1. Introduction

The term "integral abutment bridge (IAB)" usually refers to jointless bridges with short stub abutments that are rigidly connected to the superstructure without expansion joints. This rigid connection allows the abutment and the superstructure to act as a single structural unit (Arsoy *et al.* 2002). The behavior of the IAB is determined by the influence of various factors-including temperature loads, the interaction between soil and pile, and non-linear behaviors of the original ground and backfill materials-that result from the structural characteristics of a superstructure connected with the substructure without expansion joints. In particular, for the case of an IAB using a pre-stressed concrete (PSC) girder, its time-dependent characteristics have a considerable influence on the behavior of the abutment (Kim and Laman 2013, Olson *et al.* 2013). Various theoretical, numerical, and experimental studies have been conducted to determine the behavior of this type of IAB (Albhaisi and Nassif 2016, Breña *et al.* 2007, Dicleli and Albhaisi 2003, Dicleli and Albhaisi 2004, Dicleli and Erhan 2008, Dicleli and Erhan 2010, Dicleli and Erhan 2015, Fennema *et al.* 2005, Karalar and Dicleli 2016, Kim *et al.* 2009, Kim *et al.* 2012, Kim and Laman 2010, LaFave *et al.* 2016). In addition, it is necessary to identify cyclical changes in the horizontal earth pressure by performing long-term measurements on existing bridges as well as experiments at a real scale (Civjan *et al.* 2007, Lemnitzer *et al.* 2009, Nam and Park 2007, Park and Nam 2007).

∗Corresponding author, Senior Researcher
E-mail: moonsnam@gmail.com
[a]Postdoctoral Researcher
E-mail: xlage0@naver.com

The removal of expansion joints in IABs improves their drivability. However, the integration of superstructure and substructure results in an excess of member force on the pile foundation. In recent years, researchers have investigated possible ways to reduce these forces in order to increase the length of IABs (Arsoy *et al.* 2004, Dicleli and Albhaisi 2003, Feldmann *et al.* 2010). On the other hand, a fill in front of the abutment is needed to prevent lateral displacement as well as to support the pile foundation; therefore, these have the disadvantages of a bridge with a longer length and a reduced space beneath it. The expansion of the superstructure can produce an excessive passive earth pressure, which in turn (KECRI 2009, Lemnitzer *et al.* 2009, Park and Nam 2007). The differences between the non-compacted backfill and the compacted fill can cause local deformation, resulting in settlement of the approach slabs.

To overcome these problems associated with IABs, Nam *et al.* (2016) developed the integrated and pile-bent abutment with mechanically stabilized earth wall (IPM) bridge by combining the advantages of the IAB and the mechanically stabilized earth abutment bridge. The superstructure of an IPM bridge is integrated with the abutment, and the vertical load of the superstructure and its lateral displacement are supported by the pile foundation, as in a typical integral abutment. However, in an IPM bridge, the horizontal earth pressure is resisted by the mechanically stabilized earth wall (MSEW), and therefore, no earth pressure acts on the integral abutment and partially protruded piles, as shown in Fig. 1. By separating the earth pressure from the abutment, neither the fill in front of the abutment nor the non-compacted backfill are needed. Furthermore, the piles in an IPM bridge form a pile bent, and the protruded piles from the ground surface allows for less interaction with the member force of the piles' heads

http://www.techno-press.org/?journal=gae&subpage=7 ISSN: 2005-307X (Print), 2092-6219 (Online)

than in the case of an IAB. Hence, considering these issues, structural and parametric analyses were performed to determine the behavior of an IPM bridge.

2. Outline of the analysis

To determine the behavior of an IPM bridge, a structural analysis and a parametric study were conducted using a software for structural analysis, MIDAS Civil 2012 (MIDAS (2012). The behavior of the IPM bridge was expected to be similar to that of an IAB, and the conditions and parameters of the analysis were selected as in the structural analysis presented in previous studies (Ahn *et al.* 2010, Albhaisi and Nassif 2016, Dicleli and Albhaisi 2003, Dicleli and Albhaisi 2004, Kim and Laman 2010, Kim and Laman 2013, LaFave *et al.* 2016, Olson *et al.* 2013). In the case of an IAB, the lateral displacement of the superstructure is resisted by the pile foundation, and the length of the bridge is determined by the member force acting on the pile. The interaction between soil and pile has a significant influence on the bridge behavior. In this study, the behavior of the IPM bridge considers the shape of the bridge, including its length and skew, as well as the soil stiffness. Unlike an IAB, the IPM bridge is characterized by the protrusion of the piles from the ground surface, and therefore, the protruded pile length is also taken into consideration. In relation to load conditions, we took into consideration the dead loads, live loads, temperature loads, and time-dependent loads, such as drying shrinkage and creep.

The IPM bridge that was used for the structural analysis was designed in compliance with the IPM Bridge Design Guidelines (KEC 2016), which are based on(AASHTO (2002); AASHTO (2012)), VTrans (2008), KECRI (2009), MLTMA (2008), and MLTMA (2012). The design procedure for the IPM Bridge presented in the IPM Bridge Design Guidelines (KEC 2016) are a total of nine steps. From the review of the planning and application conditions of the bridges, the MSEW, the pile-bents, and the bridge piers, which are the superstructure and the substructures constituting the bridge, are individually designed. Finally, the 3D structure analysis with integrated superstructure and substructure is performed as described in this study. The IPM Bridge determines the height of the MSEW and finally determines the protuded height of the pile bent according to the bridge's longitudinal plan, unlike the conventional reverse T-type abutment. Further details of the design of the IPM bridge can be found in the IPM Bridge Design Guidelines (KEC 2016).

Fig. 1 is an IPM Bridge designed according to the IPM Bridge Design Guidelines (KEC 2016). In the general IAB, the earth pressure on the abutment is an important design factor. However, the earth pressure is supported by the MSEW, so the earth pressure does not act to the abutment and the abutment and piles are protruded on the ground surface. Fig. 1 presents each structural member of the IPM bridge and detailed descriptions are as follows.

A PSC girder, with the standard length of 30.0 m defined by the Korea Expressway Corporation (KEC), was used in the superstructure of the IPM bridge. This girder is

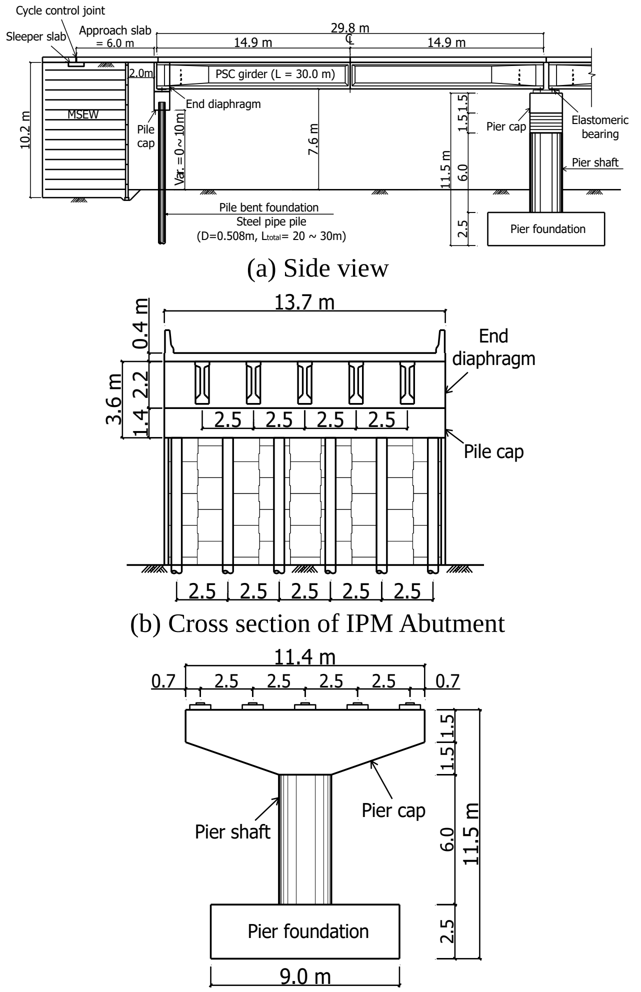

(a) Side view

(b) Cross section of IPM Abutment

(c) Cross section of pier

Fig. 1 Cross Section of IPM Bridge

Table 1 Parameter study for the structural analysis

Bridge shape	Total length (m)	30 (Single span)	60 (2 Span)	90 (3 Span)	120 (4 Span)	
	Skew (°)	0	15		15	
Protruded height of pile bent (m)		0	2	4	6	8	10
Ground stiffness	N value	10	20	30	40	50
	k_h (kN/m^3)	7,790	16,738	26,182	35,964	46,004

Table 2 Properties of the IPM abutment bridge used in the analyses

Properties	Grade	E (MPa)	υ	α(1/℃)	γ (kN/m^3)	Section
Concrete	C40	29,980	0.18	1.0×10^{-5}	24.52	Girder
	C27	26,680	0.18	1.0×10^{-5}	24.52	Plate Abutment Approach slab
Steel	STK490	205,000	0.3	1.2×10^{-5}	76.98	Pile

the most commonly constructed along expressways in Korea. Ahn *et al.* (2010) used the same PSC girder to evaluate the behavior of an IAB, although their study considered the interaction between the height of the end diaphragms, temperature changes, and earth pressures on the abutment.

The cross section of the bridge had a width of 13.4 m. Since the horizontal earth pressure was isolated from the abutment and resisted by the MSEW, it was not taken into consideration in the analysis. In accordance with the IPM Bridge Design Guidelines (KEC 2016), the length of a concrete bridge cannot exceed 120.0 m, and the skew angle is limited to 30°. In this study, the parameters for the bridge shape were selected considering these limiting conditions, and thus, the length was 30.0 m with a single span, 60.0 m with two spans, 90.0 m with three spans, and 120.0 m with four spans. As each span was added, it was regarded as part of a continuous bridge for the structural analysis. Furthermore, skew angles of 0°, 15°, and 30° were selected in this study as summarized in Table 1.

Concerning the substructure, the bridges with a single span length of 30.0 m are supported only by the IPM abutments, while those bridges with more than 30.0 m and multiple spans have concrete piers. In those cases, T-shape concrete piers are used, considering the bridge height. The abutment of the IPM bridge consisted of a pile cap and an end diaphragm, as seen in Fig. 1 (b). The pile cap basically plays the role of pile bent cap. Following the IPM Bridge Design Guidelines (KEC 2016), the structural analysis and design were performed for the dead loads of the superstructure, such as girders and bridge deck, before the superstructure was integrated with the substructure. The end diaphragm integrates the superstructure with the pile cap and the approach slab.

In the case of an IAB, given the continuous cyclic expansions that occur on the end diaphragm integrated with the superstructure, the abutment must resist the resulting earth pressure. Such earth pressure on the abutment has been a major research concern (Ahn *et al.* 2010, Dicleli and Albhaisi 2003, Nam and Park 2007, Park and Nam 2007). However, the earth pressure acting on the IPM bridge abutment is removed completely by the MSEW, so the abutment of the IPM bridge plays the relatively simpler role of combining the superstructure with the substructure. Therefore, the interaction between abutment and earth pressure was not considered in the structural analysis, and the approach slab was designed as a simple beam that spanned the abutment and support slabs, as suggested in KECRI (2016).

Steel pipe piles with a diameter of 508 mm and a thickness of 12 mm were used as pile bents. In the case of an ordinary IAB, the H-sections are aligned along the weak axis to secure flexibility for the lateral displacement of the superstructure (Albhaisi and Nassif 2016, Dicleli and Albhaisi 2003, Dicleli and Albhaisi 2004, Dicleli and Erhan 2008, Dicleli and Erhan 2015, Fennema *et al.* 2005, Kim and Laman 2010). However, if an angle exists in a bridge, the superstructure can rotate due to thermal expansion, and a subsequent distortion can take place on the H-sections. Another disadvantage is that it is difficult to place H-sections in the right position along the direction of the weak axis. For this reason, KEC (2016) used steel pipe piles instead. Therefore, the structural analysis in this study involved a model with steel pipe piles. The penetration depth of the pile bent was 20.0 m, assuming point bearing piles that penetrated a firm support layer.

Unlike an IAB, the IPM bridge has a protruding pile as a pile bent, and therefore, the behavior of the pile bent may vary depending on the protruded pile length. A parametric study on the protruded pile length under a total of six different conditions was conducted, with a protruded pile length from 0.0 m up to 10.0 m with increments of 2.0 m, as summarized in Table. 1. The IPM Bridge Design Guidelines (KEC 2016) requires that the minimum protruded pile length should be determined considering a car or train clearance, but for a comparative analysis with the IAB, the minimum protruded pile length was set as 0.0 m.

The soil stiffness was evaluated as a parameter for the ground conditions based on the Standard Penetration Test (SPT) N-values from 10 to 50. The horizontal modulus of subgrade reaction depending on the different levels of ground stiffness can be seen in Table 1, and the related estimation and verification processes will be explained in the next chapter.

3. Analysis model and conditions

3.1 Properties of the Materials

The material properties of the IPM bridge were divided into concrete and steel. The material for the PSC girder was concrete with a specified compressive strength at 28 days of 40.0 MPa, while the abutment, bridge deck, and approach slabs were made of concrete with a specified compressive strength at 28 days of 27.0 MPa. The steel pipe pile used as the pile bent was made of steel as STK490, as specified by the Korean Bridge Design Code (Limit State Design) (MLTMA 2012) with an elasticity modulus of 205,000 MPa. The properties of the materials are shown in Table 2, where E is the modulus of elasticity, ν is Poisson's ratio, α is the thermal expansion coefficient, and γ is the unit weight.

3.2 Modeling

The structural analysis model of the IPM bridge shown in Fig. 2 was determined by the design blueprint in Fig. 1 and a review of previous studies (Ahn *et al.* 2010, Albhaisi and Nassif 2016, Dicleli and Albhaisi 2003, Dicleli and Albhaisi 2004, Kim and Laman 2010, Kim and Laman 2013, LaFave *et al.* 2016, Olson *et al.* 2013). In the analysis model, girders, abutments, and piles were joined by rigid links to simulate an integral abutment. In order to consider a realistic behavior of the soil-structure interaction, nonlinear soil springs were applied to the interfaces between soil and piles. A P-y curve (Reese *et al.* 1974) was applied as the nonlinear soil springs to the interaction between soil and piles. For the interaction between the MSEW and the approach slabs, the soil spring was applied in a vertical direction, using the spring stiffness suggested by the Expressway Construction Guide Specification (KEC 2012).

The elements of the structural members and the boundary conditions of the IPM bridge were applied as follows. The girder of the superstructure was taken as a beam element, while the bridge deck and approach slabs were assumed as plate elements. The abutments, piers, and piles of the substructure were applied as beam elements. The P-y curves along the piles were applied as a multi-linear spring to simulate the yield behavior of the soil. The approach slabs and the MSEW were simulated as the surface spring support(Olson *et al.* 2009). Rotation was allowed using a hinge bar between the approach slab and the abutment, which was simulated as the plate and release option. The plate and release option is a function to input the connection conditions of the plate element, so that the bending moment of the connection between the bridge deck and the abutment connection can be eliminated. This function simulates the hinge bar. The elastic bearings of the bridge were simulated by applying elastic links.

The dimensions of the elastic bearings are as follows. Unlike abutments that are integrated with the superstructure, piers support girders with elastic bearings. The dimensions of the elastic support are as follows: capacity of 1,350 kN; a width of 300 mm, a length of 400 mm, and a height of 89 mm; compression spring coefficient of 333.4 kN/m; shear spring coefficient of 1,840.0 kN/m; and allowable displacement in the case of earthquakes of ± 90 mm. Bridge bearings were deployed to transfer the loads from the superstructure to the substructure without difficulty, and these were investigated in the 3D structural analysis. The purpose of this study was to determine the behavior of the IPM bridge, and thus, the bridge bearings installed at the piers were set up to be operable in all directions.

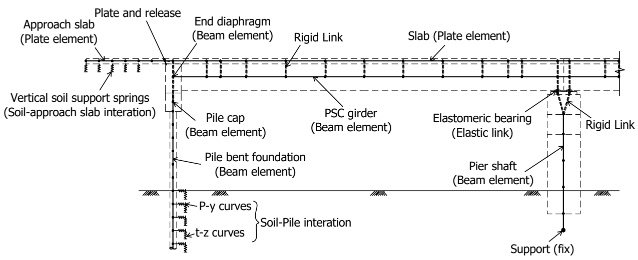

(a) Numerical model

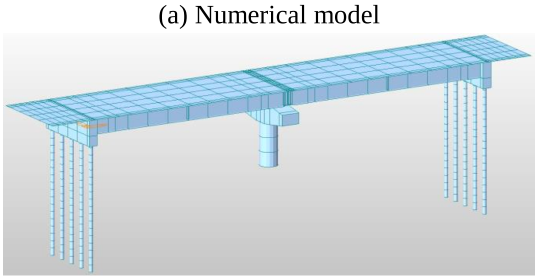

(b) 3D model (2-span bridge)

Fig. 2 Structural analysis model for IPM bridge

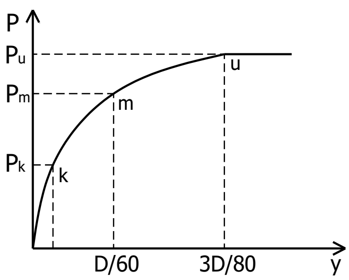

Fig. 3 P-y curve (Reese *et al.* 1974)

Table 3 P-y Curve parameters for multi-linear spring option in MIDAS Civil 2012+

Soil type	GL (m)	D (m)	γ_t(kN/m^3)	K_0	
Cohesionless soil	0.0	0.508	19.0	0.5	
N-value	E_0 (kN/m^2) E_0=700N	k_h(kN/m^3)	Ø (°) Ø $=\sqrt{12N}+20$	D_r (%)	k_1 $\left(kN/m^3\right)$
10	7,000	7,790	30.95	Loose	5,430
20	14,000	16,738	35.49	Medium	16,290
30	21,000	26,182	38.97		
40	28,000	35,964	41.91	Dense	33,930
50	35,000	46,004	44.49		

3.2.1 Modeling of P-y curve

As displacement of a pile increases, soil around the pile deforms within an elastic condition and finally reaches a yield condition. Considering this nonlinear behavior in the interaction between soil and pile, the P-y curve (Reese *et al.* 1974) was applied in this study, as shown in Fig. 3. This method has the advantages of being able to reflect a nonlinear behavior of soil, the depth-related changes in the spring coefficient, and the layered soil condition. In this study, the P-y curve of a sandy soil was applied.

The structural analysis in this study was conducted with MIDAS Civil 2012 by setting the interaction between pile and soil as the boundary condition option of the integral bridge, and the Multi-Linear Spring is used to simulate the P-y curve. The required input values can be seen in Table 3. The ground condition consisted of a sandy soil, the diameter of the pile was 508.0 mm, the total unit weight was $19.0\ \mathrm{kN/m^3}$, and the coefficient of the horizontal earth pressure (K_0) was 0.5. The modulus of elasticity of soil to model the P-y curve was defined as E_0; the horizontal modulus of subgrade reaction was defined as k_h; the internal friction angle of soil was defined as Ø; the relative compaction was defined as D_r; and the initial horizontal modulus of subgrade reaction was defined as k_1 value.

The modulus of elasticity of soil (E_0) is usually taken as $E_0 = 2800\ \mathrm{N}$ (kPa) ,where N is a SPT N-value, as suggested by the Structure Foundation Design Standards Specification (KGS 2009). However, it is commonly used in South Korea regardless of soil type. Kim *et al.* (2013) conducted a study to determine the cause of the horizontal displacement of an abutment, and suggested as modulus of elasticity of soil $E_0 = 700\ \mathrm{N}$ (kPa).

The modulus of horizontal subgrade reaction (k_h) was calculated using Eq. (1), as suggested by the Structure Foundation Design Standards Specification (KGS 2009).

$$k_h = 1.208 \cdot (\alpha \cdot E_0)^{1.103} \cdot D^{-0.281} \cdot (EI)^{-0.103} \qquad (1)$$

where α is a coefficient that depends on how the modulus of elasticity of soil is measured, D is the diameter, and EI is the flexural stiffness of the steel pipe pile.

The internal friction angle of soil was estimated by using the Dunham equation (Dunham 1954), which represents the correlation between the SPT N value and the internal friction angle of soil. The relative compaction

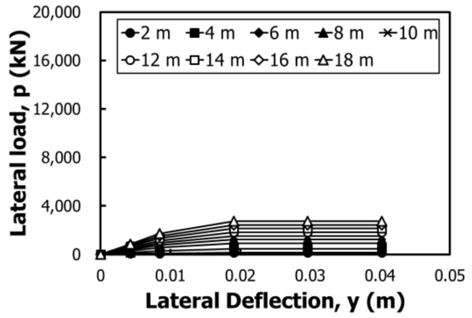

(a) $N = 10, k_h = 7{,}790\ (kN/m^3)$

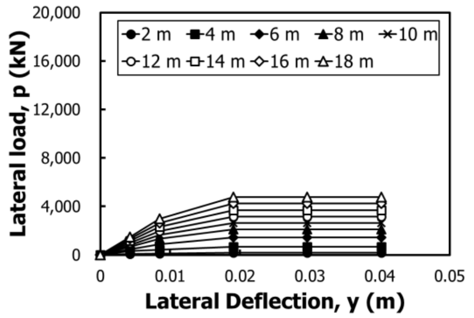

(b) $N = 20, k_h = 16{,}7380\ (kN/m^3)$

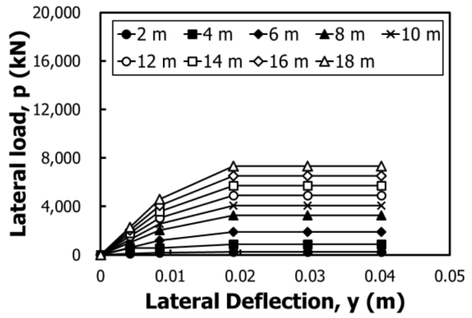

(c) $N = 30, k_h = 26{,}182\ (kN/m^3)$

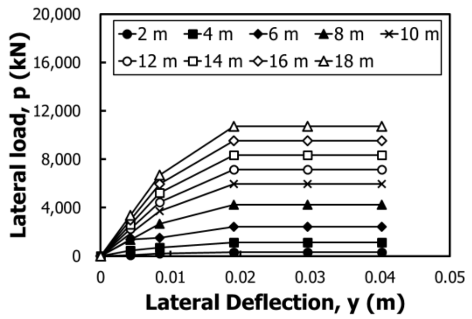

(d) $N = 40, k_h = 35{,}964\ (kN/m^3)$

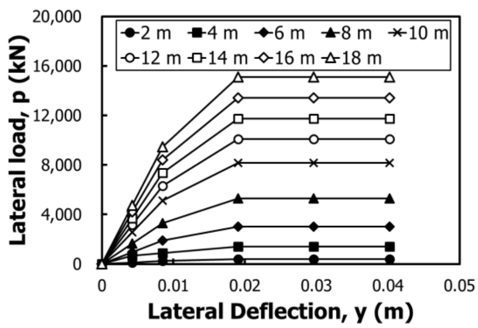

(e) $N = 50, k_h = 46{,}004\ (kN/m^3)$

Fig. 4 Multi-linear spring based on soil conditions

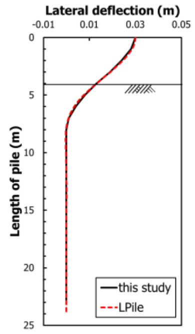

(a) Lateral displacement

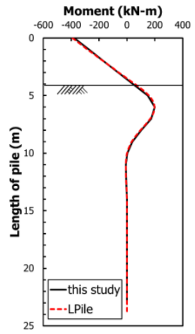

(b) Bending moment

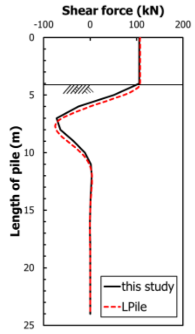

(c) Shear force

Fig. 5 Verification of P-y Curves

levels were divided into several categories, from loose to dense, depending on the inner friction angle of the sandy soil. The horizontal modulus of subgrade reaction (k_1) was estimated depending on the relative compaction level. Table 3 shows the parameters such as SPT N-values, E_0, k_h, $\emptyset$, D_r, and k_1 to develop a p-y curve using the multi-linear spring option in MIDAS Civil 2012 (MIDAS 2012). Fig. 4 shows the results of the estimation of the P-y curve by using the boundary condition options of the integral bridge in MIDAS Civil 2012 and applying the ground conditions in a Multi-Linear Spring.

The P-y curve developed with the Multi-Linear Spring in the MIDAS Civil 2012 was compared and verified using LPile Ver. 5.0 of Ensoft (Reese *et al.* 2004, Reese and Wang 2006), a commercial program that is the most commonly used in the world for P-y analyses. The conditions used in the comparison and verification analysis were modeled by setting the total pile length at 24.0 m, the penetration depth at 20.0 m, and the protruded pile length at 4.0 m. The ground conditions were assumed to have a SPT N-value of 20, as suggested in Table 3. The load conditions exerted a displacement in the horizontal direction of 30.0 mm, and the boundary conditions of the pile head were fixed. Fig. 5 shows the pile behaviors obtained in this study (MIDAS Civil 2012) and using LPile Ver. 5.0. The lateral deflection, the bending moment, and the shear strength were estimated in the same manner.

The t-z curve representing the tangential behavior of the pile was simulated with a linear elastic spring. The reason why the p-y curve representing the lateral behavior is simulated by the nonlinear elastic spring and the t-z curve representing the vertical behavior is simulated by the linear elastic spring is as follows. First, the IPM Bridge and IAB are dominated by the behavior of the pile and the entire bridge in the lateral displacement of the superstructure. The pile-bent of the IPM Bridge presented in Fig. 1 is designed to support the vertical load of the superstructure within the elastic region. Therefore, the t-z curve is simulated with a linear elastic spring, and the stiffness is calculated as shown in Eq. (2).

$$k_{tan} = D \cdot K_0 \cdot \gamma \cdot x \cdot \tan \phi' \quad (2)$$

where, D is the diameter of the pile (m), K_0 is the earth pressure coefficient at rest, γ is the unit weight of the soil, x is the depth from the surface (m), and ϕ'' is the internal friction angle of the soil (°).

3.2.2 Modeling of the soil-approach slab interaction

In the IPM bridge, the horizontal earth pressure and the approach slab loads are supported by the MSEW. Hence, the interaction between the upper side of the MSEW and the approach slabs must be considered. This is a vertical interaction, which is different from that between MSEW and piles, and it is simulated as the surface spring support among the boundary condition options offered by MIDAS Civil 2012. The stiffness of the surface spring support was estimated into vertical soil reaction coefficients, which are calculated according to the soil conditions.

The Structure Foundation Design Standards Specification (KGS 2009) provides the relation between the SPT N=value and the vertical ground reaction coefficient $k_{0.3}$ for a 0.3 m of diameter foundation of the plate bearing test (ASTM 1994), as seen in Eq. (3).

$$k_{0.3}(kN/m^3) = 1{,}800N \text{ (Scott 1981)} \quad (3)$$

To use them as vertical soil reaction coefficients, they need to be modified considering the length and width of the approach slabs. The vertical soil reaction coefficient ($k_{0.3}$) with a diameter of 0.3 m suggested in Eq. (3) was modified into the initial vertical soil reaction coefficient with a square sized foundation (k_{BB}), as seen in Eq. (4).

$$k_{BB} = k_{0.3}\left(\frac{B+0.3}{2B}\right)^2 = k_{0.3}\left(\frac{6+0.3}{12}\right)^2 = 0.525 \times k_{0.3} \quad (4)$$

The initial vertical ground reaction coefficient with a size of B (m) × B (m) (k_{BB}) was again modified considering the length and width of the approach slab into the initial vertical ground reaction coefficient with a rectangular sized foundation (k_{BL}), as seen in Eq. (5).

$$k_{BL} = \frac{k_{BB}\left(1+0.5\frac{B}{L}\right)}{1.5} = \frac{k_{BB}\left(1+0.5\frac{6.0}{12.0}\right)}{15} = \frac{1.25k_{BB}}{1.5} = 0.833 \times k_{BB} \quad (5)$$

where B is the width of an approach slab, and L is the length. The approach slab of the IPM bridge designed in this study is 6 m in width and 12 m in length.

The approach slab of the IPM bridge was constructed on the MSEW. In this study, k_{BL}=19687.5(kN/m^3) at N=25 was applied according to the Expressway Construction Guide Specification (KEC 2012).

3.3 Loading Conditions

To determine the behavior of the IPM bridge, several load conditions were considered, including dead loads; live loads induced by temperature variation and vehicles traveling; and time-dependent loads such as drying shrinkage, creep, and temperature. The influence of the relaxation of a PSC girder's stranded cable, which is a time-dependent load that affects the girder's behavior, was not considered.

Table 4 Temperature ranges and thermal expansion coefficient (MLTMA 2008)

Bridge type	Temperature ranges		α (1/℃)
	Moderate	Cold	
Concrete bridge	−5 to 35℃	−15 to 35℃	1.0×10^{-5}
Steel bridge (Upper route bridge)	−10 to 40℃	−20 to 40℃	1.2×10^{-5}
Steel bridge (Lower route bridge and Steel deck bridge)	−10 to 50℃	−20 to 40℃	1.2×10^{-5}

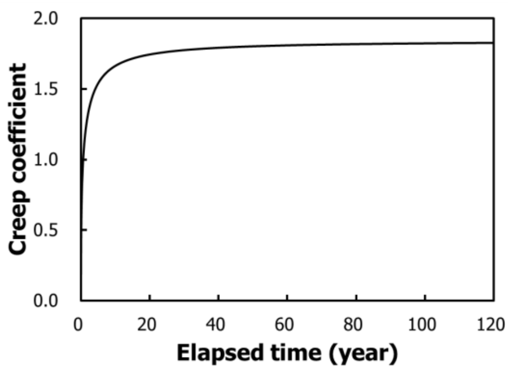

(a) Creep coefficient

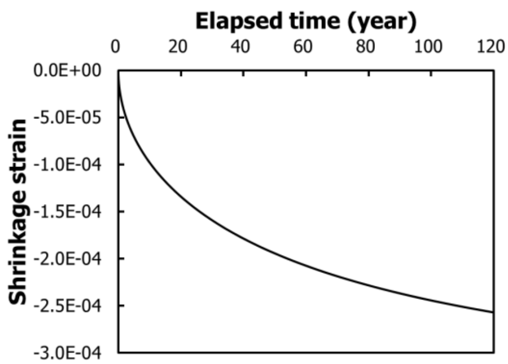

(b) Shrinkage strain

Fig. 6. Time-dependent loads (Drying shrinkage and creep)

The dead load was calculated by applying the acceleration speed in the gravitational direction in MIDAS Civil 2012. Dead loads were applied to the barrier that was not included in the structural analysis modeling. The live loads suggested by AASHTO (2002) and KRA (2012) were applied as live loads and were modeled with MIDAS Civil 2012.

The temperature load induced by temperature variations was applied with the temperature changes and thermal expansion coefficient (α) suggested in the Bridge Design Specifications (KRA 2012) as summarized in Table 4. Here, the PSC bridge was selected as the bridge type, and the thermal expansion coefficient (α) was 1.0×10^{-5}(1/℃). Regarding the temperature change, a cold climate region in Korea with a temperature range of -15 to 35℃ was applied. South Korea's average autumn temperature of 10℃ was set as the installation temperature. Several studies have been conducted considering the thermal changes on the IABs (Dicleli and Albhaisi 2004, Kim and Laman 2010, 2013), but this study only applied the temperature loads to the IPM bridge. The placing temperature of concrete was 10℃, but was set at -25℃ during the winter and at +25℃ during the summer.

Regarding the time-dependent loads such as drying shrinkage and creep, it was applied the CEB-FIP (1990) model code suggested by the Bridge Design Specification (KRA 2012). The PSC girder's compression strength at 28-day was assumed as 40 MPa, the ambient temperature of 70% and geometric dimensions of 1.2 m were applied. Normal Portland cement was chosen, and the starting time for drying shrinkage after cement placing was set to 3-day. Fig. 6 shows the change of the drying shrinkage and creep coefficients, which are time-dependent loads. In this study, a stage analysis was performed to analyze the time-dependent behavior. The analysis was conducted based on a 120-year service life or 20 years plus the 100-year standard service life of Korean expressways. As shown in Fig. 6(a), the creep coefficient over the time lapse stabilizes after about 20 years. As seen in Fig. 6(b), the dry shrinkage-induced strain rate was reduced to approximately -2.5×10^{-4} after 120 years.

3.4 Analysis stage

The structural analysis of the IPM bridge was performed using four methods of analysis: static analysis induced by self-weight and dead loads; live load analysis induced by live loads; temperature analysis induced by temperature loads; and, construction stage analysis of a 120-year service life to assess the influence of time-dependent loads, such as drying shrinkage and creep.

4. Analysis results

To determine the behavior of the IPM bridge, it was considered the influence of several loading conditions for different bridge lengths and skew angles. Finally, the influence of the protruded length of the pile bents and the soil stiffness in the bridge behavior was identified. The results of the structural analysis were based on the head of the pile-bent. The reason for this is that, the greatest force was developed on the pile head under the condition of fixed head and supporting the lateral load. This is the same as the experimental and numerical results for the previous studies on the IAB (Dicleli 2000, Dicleli and Albhaisi 2004, Feldmann *et al*. 2010).

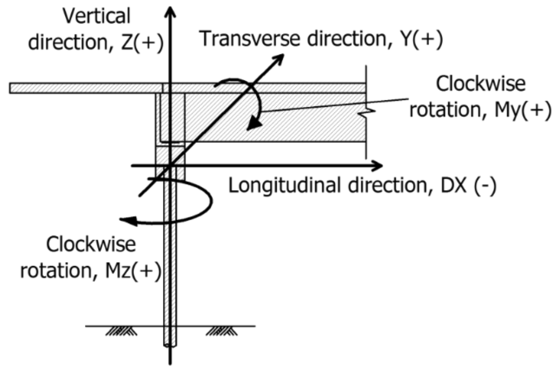

Fig. 7. Sign Convention

Before considering the results of the analysis, a sign convention was defined as shown in Fig. 7. The displacement in the longitudinal direction had a negative (-) value when it shrunk along the X-axis, and it had a positive (+) value when it expanded toward the back face of an abutment. The displacement in the transverse direction had a positive (+) value when it occurred on the left side or had a negative (-) value when it occurred on the right side. Regarding the moments acting on the pile bents, the moment in the same direction as the rotation direction of the girder of the superstructure was defined as My, which had a positive (+) value when it occurred in the clockwise direction or a negative (-) value when it occurred in the counter-clockwise direction. The moment causing torsion on the foundation of pile bents was defined as Mz, which had a positive (+) value when it occurred in the clockwise direction or had a negative (-) value when it occurred in the counter-clockwise direction.

4.1 Influence of loading conditions depending on different bridge lengths

Fig. 8 shows the results of the structural analysis of the loading conditions depending on the length of the bridges. The skew angle of the bridge was set to 0°, the protruded pile lengths was set to 4.0 m, and the soil stiffness was set at SPT N value as 20. Fig. 8(a) shows the bending moment (My) working on the pile head. The highest level of the bending moment (My) was caused by drying shrinkage (SH), temperature increase (TL+), and temperature decrease (TL-), being followed by the 1st dead loads (1st DL) and creep (CR). Fig. 8(b) showed a bending moment (Mz) working as torsion on the pile head. It is significantly influenced by the temperature load, but it was not influenced by the bridge length. Fig. 8(c) shows the displacement in the longitudinal direction (DX). Like the bending moment working on the pile head, the highest level of displacement was caused by the drying shrinkage (SH), temperature increase (TL+), and temperature decrease (TL-). Fig. 8(d) showed the displacement in the transverse direction (DY). The DY was about 20 times lower than the DX. Unlike the bending moment (My) working on the pile head and the displacement in the bridge axis direction (DX), the live load (LL) showed the greatest influence, followed by the temperature increase (TL+) and temperature decrease (TL-). However, the drying shrinkage (SH) and creep (CR) had almost no influence. Moreover, the displacement in the transverse direction was not significantly influenced by individual loads.

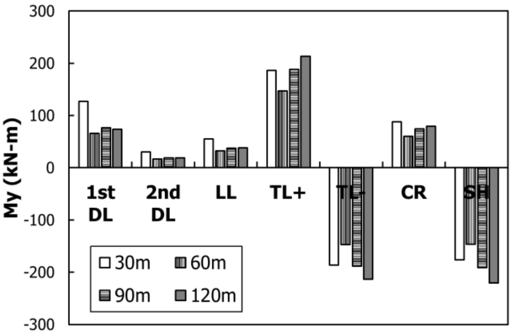

(a) Bending moment, My

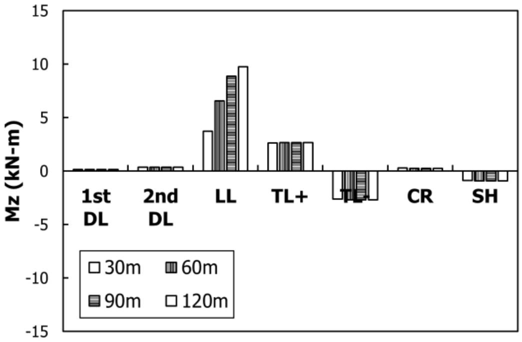

(b) Bending moment, Mz

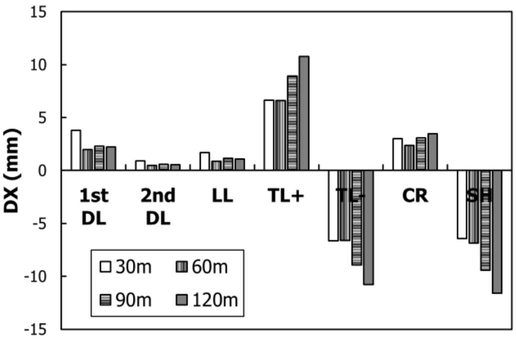

(c) Longitudinal displacement, DX

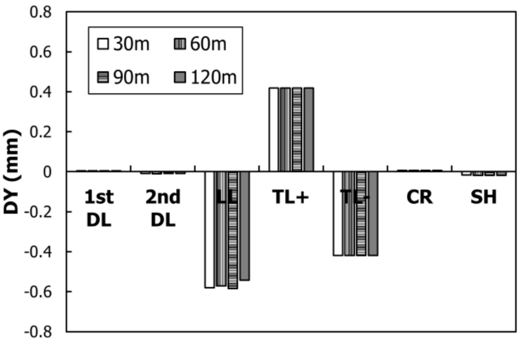

(d) Transverse displacement, DY

Fig. 8 Influence of loading conditions depending on different bridge lengths

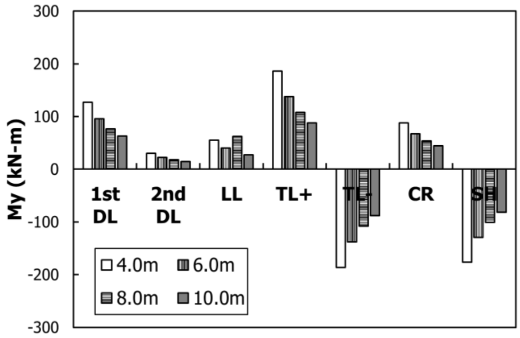

(a) Bending moment, My

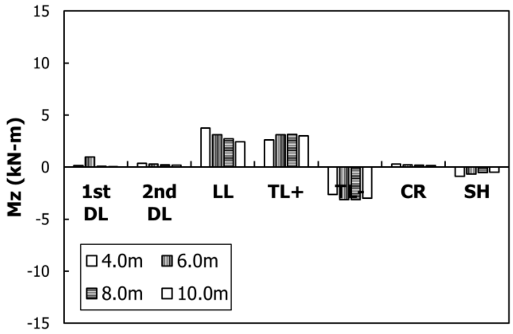

(b) Bending moment, Mz

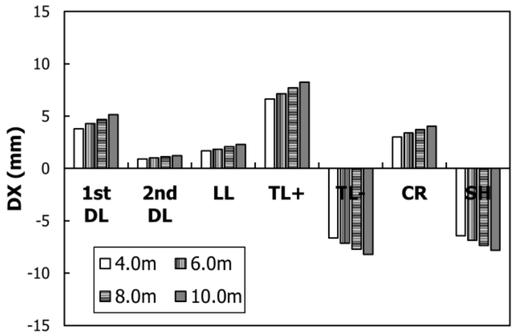

(c) Longitudinal displacement, DX

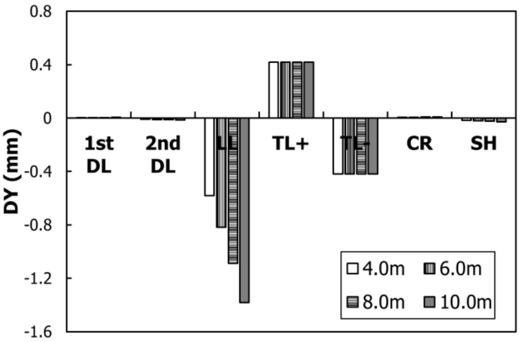

(d) Transverse displacement, DY

Fig. 9 Influence of loading conditions depending on different protruded pile lengths

4.2 Influence of loading conditions depending on different protruded pile lengths

Fig. 9 shows the results of the structural analysis of the working loads depending on the protruded pile lengths. Here, the length of the bridge was 30 m, the skew angle was set to 0°, and the ground stiffness was set at SPT N value as

20. The working loads acting on the member force and the displacement of the pile bent were estimated in the same way as in Fig. 8. With an increase in the protruded pile lengths, the bending moment in the bridge axis direction (My) caused by individual loads showed a declining tendency, and the displacement in the longitudinal direction (DX) had an increasing tendency. However, the bending moment in the torsional direction and the displacement in the transverse direction showed variations only for the live load (LL), in accordance with the protruded pile lengths.

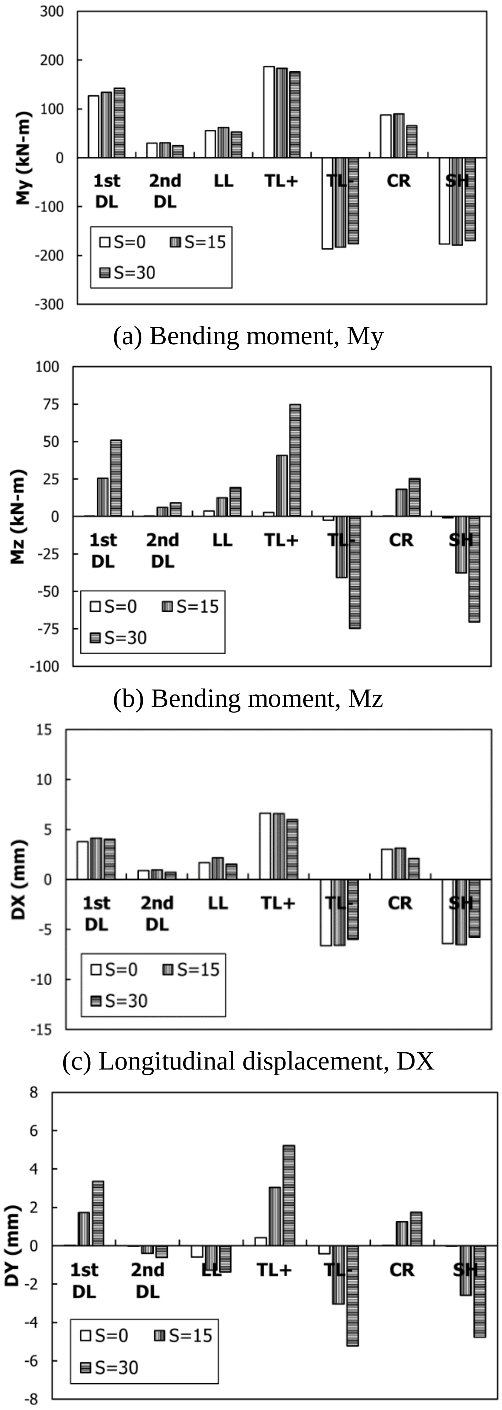

Fig. 10 Influence of loading conditions depending on different skew angles

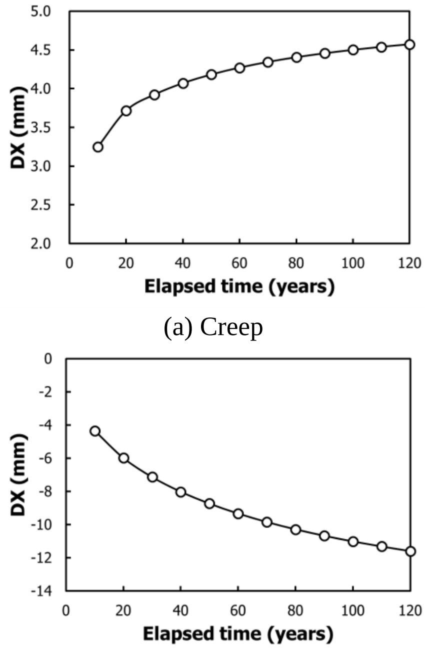

Fig. 11 Displacement in longitudinal direction (DX) caused by time-dependent loads

4.3 Influence of loading conditions depending on different skew angles

Fig. 10 shows the results of the structural analysis of the working loads depending on the bridge skew angle. As in Fig. 8, the protruded pile lengths was 4.0 m, the ground stiffness was set at SPT N value as 20, the length of the bridge was 30 m, and the skew angle was between 0° to 30°. Fig. 10(a) and 10(c) show the bending moment working on the pile head (My) and the displacement in the longitudinal direction (DX), respectively, and it can be seen that the degree of influence of the individual loads is the same as that in Fig. 8. No significant changes in the bending moment (My) and in the displacement in the longitudinal direction (DX) occurred in relation to the different skew angles. However, the bending moment in the torsional direction (Mz) and the displacement in the transverse direction suggested in Fig. 10(b) and 10(d) showed variations depending on the skew angles.

When the skew angle was 0°, the live load (LL), temperature increase (TL+), and temperature decrease (TL-) showed the greatest influence. However, when the skew angle increased to 15° and 30°, the displacement in the transverse direction (DY) was greatly influenced by the temperature increase (TL+), the temperature decrease (TL-), the drying shrinkage (SH), the 1st dead load (1st DL), and the creep (CR). In particular, when the skew angle was 30°, the bending moment (Mz) increased by about 12 times compared to when the skew angle was 0°, and the displacement in the transverse direction surged by about 12 times.

4.4 Behavior of an IPM bridge due to time-dependent loads

Fig. 11 shows the displacement in the longitudinal direction (DX) caused by the time-dependent loads. The protruded pile lengths was 4.0 m, the ground stiffness was set at SPT N value as 20, the length of the bridge was 120 m, and the skew angle was 0°. A stage analysis was conducted on time-dependent loads such as drying shrinkage and creep, considering the variation in the coefficients suggested in Fig. 6. This study analyzed the behavior for up to 120 years, considering that 100 years is the standard service life of an IPM bridge. The displacement of the pile head in the bridge axis direction caused by the drying shrinkage and the creep continued to increase, but also increasingly converged, as time lapsed. In accordance with the code protocol, when the creep in Fig. 11(a) showed an expansion in the longitudinal direction (DX), it had a negative (-) value. When the drying shrinkage in Fig. 11(b) showed a drying shrinkage behavior, it had a positive (+) value. The displacement in the longitudinal direction (DX) influenced by the drying shrinkage was about 2.5 times higher than that caused by the creep.

4.5 Behavior of an IPM bridge due to temperature loads

In an IPM bridge, the superstructure is integrated with the substructure, and an expansion can occur in the superstructure due to seasonal temperature variations. If individual loads are combined, the IPM bridge appears to show different behaviors during the summer and winter. To achieve the results of the structural analysis, this study applied a combination of individual loads suggested by AASHTO (2002): 1.3 DL + 2.15 LL + 1.3 TU + 1.3 SH + 1.3 CR. Here, the behavior of the IPM bride is analyzed by dividing the temperature load into a temperature increase (TL+) for the summer and temperature decrease (TL-) for the winter. The experimental conditions are as follows; the length of the bridge was 120 m (4 spans); the protruded pile length was 4.0 m, and the ground stiffness was set at SPT N value as 20.

Fig. 12 shows the displacement of the pile bent in the longitudinal direction (DX) in order to examine the seasonal behavior of the IPM bridge. In Fig. 12, S-1 and W-1 indicate the temperature increase (TL+) and temperature decrease (TL-), respectively, while S-2 and W-2 are the combinations of the temperature load, deal load (DL), and live load (LL). S-3 and W-3 add the time-dependent loads such as drying shrinkage (SH) and creep (CR). The temperature was set to -15℃ for the winter and +35℃ for the summer, with a temperature change within ±25℃ based on an installation temperature of 10℃.

The displacement of the pile bent in the longitudinal direction (DX) in the cases of S-1 and W-1 was ±13.92 mm, and it showed symmetry in the drying shrinkage and the expansion behavior. Here, when the dead load (DL) and the live load (LL) were applied, the deflection of the girder and the rotation of the abutment occurred, and the displacement in the longitudinal direction (DX) showed an expansion toward the back of the abutment. In S-2, the temperature increase (TL+) during the summer showed a displacement of -17.93 mm, while in W-2 the temperature decrease (TL -) during the winter showed a displacement of +11.89 mm.

In the case of an IAB, the behavior of the pile bent has

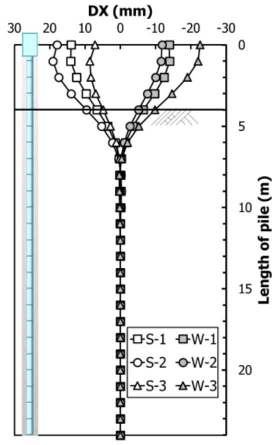

Fig. 12 Behavior of IPM bridge due to temperature loads

been known to be dominated by the rotation of the integral abutment. Many studies have been conducted to confirm this (Arsoy *et al.* 2002, Dicleli and Erhan 2008, LaFave *et al.* 2016, Olson *et al.* 2013). Olson *et al.* (2013) reported that the rotation of an abutment is dominated by the stiffness and shape of a girder. When the drying shrinkage (SH) and the creep (CR) were additionally combined, the displacement of S-3 during the summer decreased to -7.16 mm, and the displacement of W-3 increased to +22.66 mm. The time-dependent loads represented the displacement after 120 years because the drying shrinkage behavior or the SH had a significant influence.

4.6 Behavior of an IPM bridge due to different bridge and protruded pile lengths

Figs. 13 and 14 show the results of the analysis of the bridge behavior depending on the protruded pile lengths and the length of the bridge. As shown in Figs. 13 and 14, the loads were combined in accordance with load factors of 1.3 DL + 2.15 LL + 1.3 TU + 1.3 SH + 1.3 CR, as presented in AASHTO (2002), and in accordance with the temperature changes in the summer (TL+) and the winter (TL-). In this case, the skew angle of the bridge was 0°, and the ground stiffness was set at SPT N value as 20.

A comparison of the bridge behavior depending on the protruded pile length shows that the bending moment (My) in summer in Fig. 13(a) and in winter in Fig. 14(a) decreased as the height increased. In contrast, the displacement in the longitudinal direction (DX) increased in summer as shown in Fig. 13(b) and in winter as shown in Fig. 14(b). The displacement in the transverse direction (DY) in Figs. 13(c) and 14(c) also increased in accordance with the protruded pile length, but the increase was relatively smaller than that of the displacement in the longitudinal direction (DX). The result showed that the member forces decreased and the displacement increased when the protruded length of the pile increased.

The IMP bridge must have a car clearance of 4.0 m under the bridge when crossing a road and a train clearance of 7.3 m under the bridge when crossing a railway, as defined in the Bridge Design Specification (KRA 2012). The minimum height of the IPM bridge is limited to 4.0 m

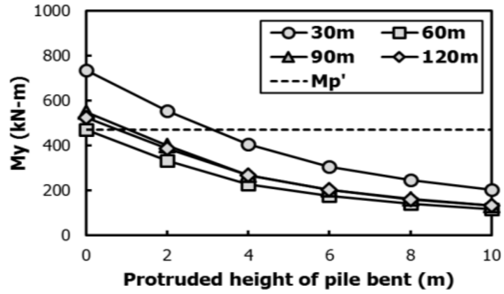

(a) Bending moment, My

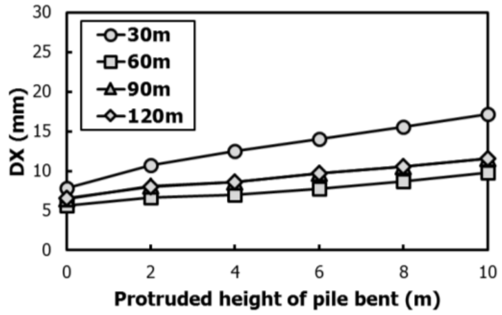

(b) Longitudinal displacement, DX

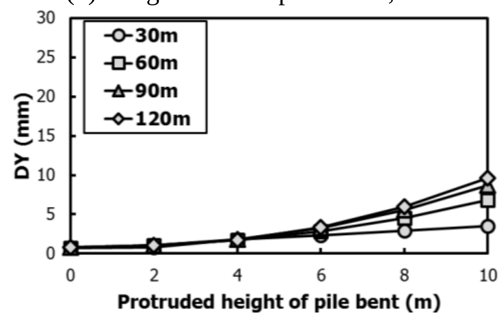

(c) Transverse displacement, DY

Fig. 13 Behavior of IPM bridge due to different bridge lengths and protruded pile lengths in summer condition

in the IPM Bridge Design Guidelines (KEC 2016). Compared to the case where the pile does not protrude from the ground surface, as with IABs, the bending moment (My) acting on the pile head was reduced by about 60%, and the displacement in the longitudinal direction (DX) increased by about 12%.

The design of IAB piles is divided into upper zone and lower zone according to load conditions. Upper zone resists both axial load and bending moment, while lower zone resists only axial load. Since the pile head in the IAB is constrained to the superstructure, the largest bending moment is generated in the pile head. The applied moment (M_u) on the pile head due to the working load should be smaller than the bending moment ($M_{p\prime}$)which causes the plastic hinge (VTrans 2008). The detailed design procedures for IAB piles can refer in Integral Abutment Bridge Design Guidelines (VTrans 2008). The pile-bent is designed as a column that simultaneously resists compression and bending, and the bending moment ($M_{p\prime}$) that generates the plastic hinge is Eq. (6).

$$M_{p\prime} = \frac{9.0}{8.0}\left(1.0 - \frac{P_u}{P_r}\right) \times M_r \tag{6}$$

where P_u is the applied axial load (kN), P_r is the calculated compressive structural pile resistance (kN), and M_r is the calculated bending moment strength (kN · m).

Based on the Eq. (6), the bending moment M_p' that generates a plastic hinge on the heads of the steel pipe pile with a diameter of 508 mm and a thickness of 12 mm is 470.1 kN · m.

The results of the analysis in Figs. 13 and 14 indicate that when the pile protruded length was 0.0-2.0 m, the bending moment (My) on the heads of the pile foundation exceeded the bending moment M_p' in which the plastic hinge was generated. As a result, and since in an IAB its extension is limited because of the excessive member force on its pile bent, the IMP bridge is an effective alternative to improve the length of an integral bridge.

Regarding the behaviors that depend on the length of the bridge, shrinkage during the winter showed a bending moment (My) and displacement in the longitudinal bridge axis direction (DX) that increased if the length of the bridge increased. It showed relatively smaller changes than with the protrusion height. However, the displacement in the longitudinal direction (DX) increased by about 270% when the length of the bridge increased from 30.0 m to 120.0 m.

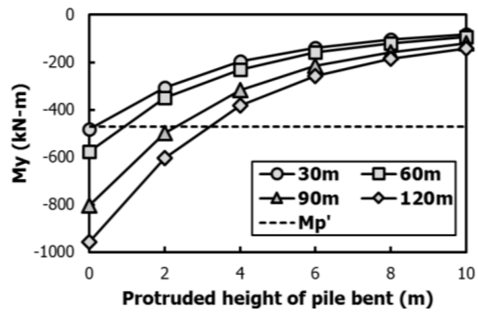

(a) Bending moment, My

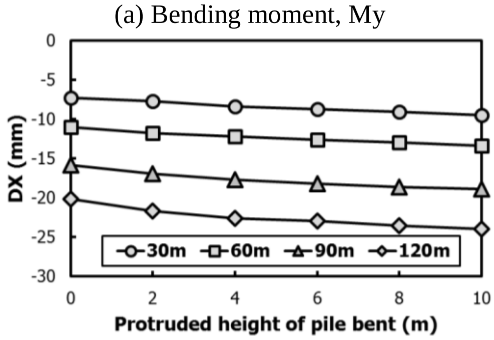

(b) Longitudinal displacement, DX

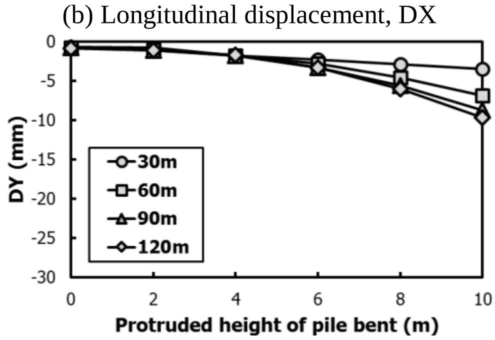

(c) Transverse displacement, DY

Fig. 14 Behavior of IPM bridge due to different bridge lengths and protruded pile lengths in winter condition

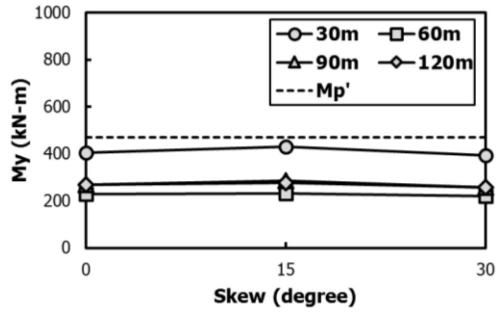

(a) Bending moment, My

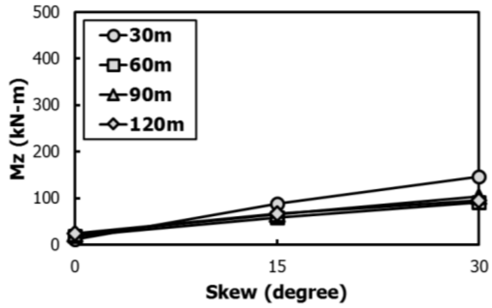

(b) Bending moment, Mz

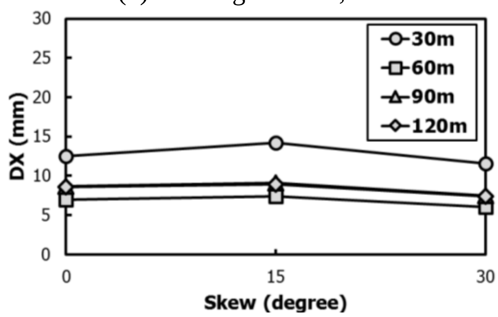

(c) Longitudinal displacement, DX

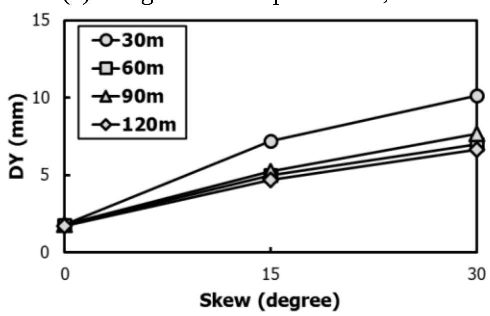

(d) Transverse displacement, DY

Fig. 15 Behavior of IPM bridge due to skew angles

4.7 Behavior of IPM bridge due to skew angles

Fig. 15 shows the result of the structural analysis in relation with the skew angle of the bridge. The protruded pile length of the pile bent was 4.0 m, and the ground stiffness was set at SPT N value as 20. The bending moment (My) in Fig. 15(a) and the displacement in the longitudinal direction (DX) in Fig. 15(c) did not show any changes related to the skew angles. However, the displacement in the transverse direction (DY) and the bending moment (Mz) in the torsional direction of the pile foundation in Fig. 15(b) increased in accordance with the skew angles. This bridge has a width of 13.4 m, for a round-trip two-lane road. However, if the bridge width increases, the impact on the skew angles will be greater, and additional research is needed on this issue. In integrated bridges, the impact of the skew angles is more complex due to the passive earth pressure on the abutment. However, IMP bridges have the advantage of being affected only by the bridge structure since the earth pressure on the abutment is removed. The IPM Bridge Design Guidelines (KEC 2016) limit the skew angle of the IPM bridges to less than 30°, to avoid a possible twist of the piles.

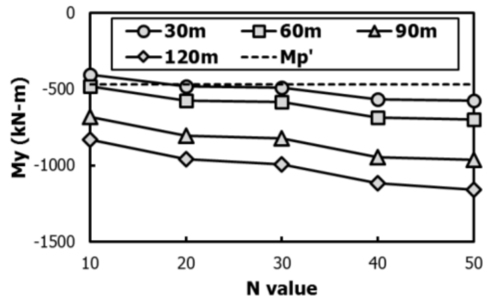

(a) Bending moment, My

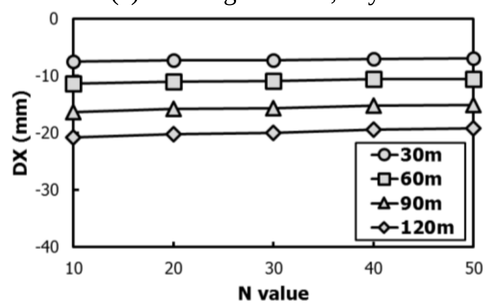

(b) Longitudinal displacement, DX

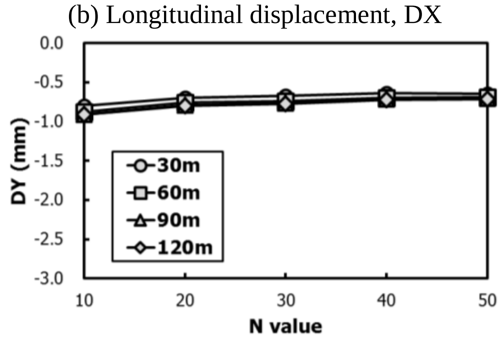

(c) Transverse displacement, DY

Fig. 16 Behavior of IPM bridge due to different soil stiffness with protruded pile lengths of 0.0 m

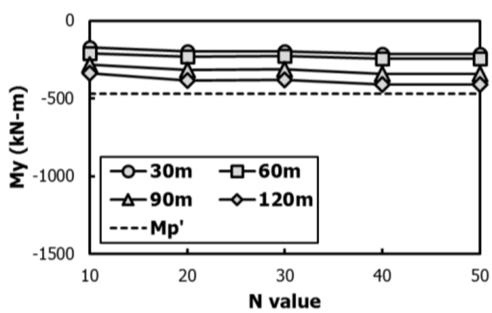

(a) Bending moment, My

Fig. 17 Behavior of IPM bridge due to different soil stiffness with protruded pile lengths of 4.0 m

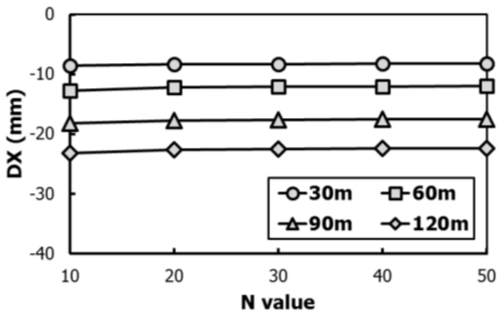

(b) Longitudinal displacement, DX

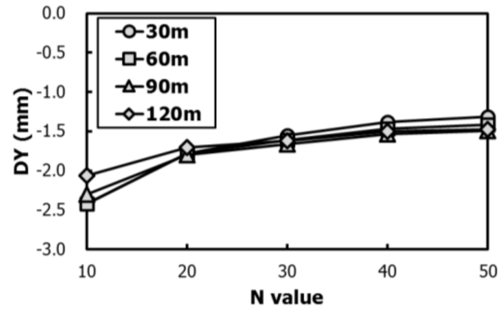

(c) Transverse displacement, DY

Fig. 17 Continued

4.8 Behavior of IPM bridge due to different soil stiffness

Figs. 16 and 17 show the result of the structural analysis in relation with the stiffness of soil around piles. The protruded pile lengths were set as 0.0 m and 4.0 m, and the soil stiffness around piles was represented as SPT values from 10 to 50. The results of the analysis only show the shrinkage behavior in the winter, where a relatively large member force acted. Fig. 16(a) and Fig. 17(a) show the bending moment (My) acting on the pile heads with protruded pile lengths of 0.0 m and 4.0 m. When the protruded pile length was 0.0 m, the bending moment (My) increased greatly if the SPT N-values increased from 10 to 50, as shown in Fig. 16(a). If the protruded pile length was 4.0 m, there were few changes in the bending moment (My) due to the ground stiffness. The displacement in the longitudinal direction (DX) in Fig. 16(b) and Fig. 17(b) was compared to the displacement in the transverse direction (DY) in Fig. 16(c) and Fig. 17(c). When the protruded pile length was 0.0 m, the effect of the ground stiffness was large. Hence, the behavior of the IMP bridges was influenced to a larger extent by the protruded pile length than by the ground stiffness. Figs. 13, 14, 16, and 17 show that the bending moment, which was exerted on the pile bent that protruded from the ground, had been greatly reduced.

Dicleli and Albhaisi (2003) compared the displacement of an IAB deck in relation with the horizontal modulus of subgrade reaction (k_h=3000-18000 (kN/m^3)). The k_h had an inflection point at 6000 kN/m^3. Based on the SPT N-values, when N was 10 then k_h=7790 (kN/m^3), which exceeded the inflection point k_h=6000 (kN/m^3), but the member force in accordance with the ground stiffness shows inelastic behavior.

5. Conclusions

The conclusions of this study are as follows:

- Both the IPM bridge and the IAB were affected the most by temperature and time-dependent loads such as creep and dry shrinkage. The temperature and time-dependent loads were superimposed on each other, and the shrinkage behavior during the winter was relatively larger than the expansion behavior during the summer.
- The IPM bridge with a partially protruded pile bent had the largest member force on the pile head, as in an IAB. It was influenced the most by the protruded pile lengths rather than by the shape of the bridge or the ground stiffness.
- Since the IAB length is limited by an excessive member force on the piles, the IMP bridge is an effective alternative to improve the length limit of an integral bridge.
- The displacement in the direction perpendicular to the bridge axis and the bending moment in the torsional direction of the pile increased in relation with the skew angles of the bridge. They are also affected by the bridge width, so additional research is needed on skew angles and bridge width.
- Comparing the IPM Bridge with the IAB, the influence factors and the behavior characteristics are the same as the integral bridges. The difference is that the IPM Bridge, which has a feature of partially protruding pile-bents, has the advantage that the member force of the pile is less than the IAB and the effect of the surrounding soil rigidity is reduced.
- The MSEW supports the approach slabs of an IPM bridge, and therefore, the settlements of the reinforced earth retaining walls may cause damage to the superstructure. Additional research is also needed on this issue.

References

AASHTO (2002), *Standard Specifications for Highway Bridges*, American Association of State Highway & Transportation Officials, Washington, D.C., U.S.A.

AASHTO (2012), *AASHTO LRFD Bridge Design Specifications*, American Association of State Highway and Transportation Officials, Washington, D.C., U.S.A.

Ahn, J.H., Yoon, J.H., Kim, S.H. and Kim, J.H. (2010), "Evaluation on behavior characteristics of PSC integral abutment bridge", *J. Kor. Soc. Civ. Eng.*, **30**(4A), 361-373.

Albhaisi, S. and Nassif, H. (2016), "Correlation between 2D and 3D analysis of integral abutment bridges", *Proceedings of the Transportation Research Board 95th Annual Meeting*, Washington, D.C., U.S.A., January.

Arsoy, S., Barker, R.M. and Duncan, J.M. (2002), "Experimental and analytical investigations of piles and abutments of integral bridges", Virginia Department of Transportation, Virginia Polytechnic Institute and State University, Blacksburg, Virginia, U.S.A.

Arsoy, S., Duncan, J.M. and Barker, R.M. (2004), "Behavior of a semiintegral bridge abutment under static and temperature-induced cyclic loading", *J. Bridge Eng.*, **9**(2), 193-199.

ASTM (1994), *Standard Test Method for Bearing Capacity of Soil for Static Load and Spread Footings*, ASTM International, West Conshohochen, Pennsylvania, U.S.A.

Breña, S.F., Bonczar, C.H., Civjan, S.A., DeJong, J.T. and Crovo, D.S. (2007), “Evaluation of seasonal and yearly behavior of an integral abutment bridge”, *J. Bridge Eng*., **12**(3), 296-305.

CEB-FIP (1990), *Model Code 1990*, Bulletin d’Information, Thomas Telford House, Lausanne, Switzerland.

Civjan, S.A., Bonczar, C., Brena, S.F., DeJong, J. and Crovo, D. (2007), “Integral abutment bridge behavior: Parametric analysis of a Massachusetts bridge”, *J. Bridge Eng*., **12**(1), 64-71.

Dicleli, M. (2000), “A rational design approach for prestressed-concrete-girder integral bridges”, *Eng. Struct*., **22**(3), 230-245.

Dicleli, M. and Albhaisi, S.M. (2003), “Maximum length of integral bridges supported on steel H-piles driven in sand”, *Eng. Struct*., **25**(12), 1491-1504.

Dicleli, M. and Albhaisi, S.M. (2004), “Effect of cyclic thermal loading on the performance of steel H-piles in integral bridges with stub-abutments”, *J. Construct. Steel Res*., **60**(2), 161-182.

Dicleli, M. and Erhan, S. (2008), “Effect of soil and substructure properties on live-load distribution in integral abutment bridges”, *J. Bridge Eng*., **13**(5), 527-539.

Dicleli, M. and Erhan, S. (2010), “Effect of soil-bridge interaction on the magnitude of internal forces in integral abutment bridge components due to live load effects”, *Eng. Struct*., **32**(1), 129-145.

Dicleli, M. and Erhan, S. (2015), *Low Cycle Fatigue Effects in Integral Bridge Steel H-Piles Under Earthquake Induced Strain Reversals*, in *Advances in Structural Engineering*, Springer, New Delhi, India. 2505-2512.

Dunham, J.W. (1954), “Pile foundations for buildings”, *Proc. Am. Soc. Civ. Eng*., 1-21.

Feldmann, M., Naumes, J., Pak, D., Veljkovic, M., Nilsson, M., Eriksen, J., Collin, P., Kerokoski, O., Pétursson, H. and Verstraete, M. (2010), *Economic and Durable Design of Composite Bridges with Integral Abutments*, Publication Office of the European Union.

Fennema, J.L., Laman, J.A. and Linzell, D.G. (2005), “Predicted and measured response of an integral abutment bridge”, *J. Bridge Eng*., **10**(6), 666-677.

Karalar, M. and Dicleli, M. (2016), “Effect of thermal induced flexural strain cycles on the low cycle fatigue performance of integral bridge steel H-piles”, *Eng. Struct*., **124**, 388-404.

KEC (2012), *Expressway Construction Guide Specification*, Korea Expressway Corperation, Hwaseong, Korea (in Korean).

KEC (2016), *IPM Bridge Design Guidelines*, Korea Expressway Corperation, Hwaseong, Korea (in Korean).

KECRI (2009), *Integral Bridge Design Guidelines*, Korea Expressway Corperation Research Institute, Hwsaseong, Korea, 1-59 (in Korean).

KGS (2009), *Structure Foundation Design Standards Specification*, Korean Geotechnical Society, Seoul, Korea (in Korean).

Kim, S.H., Yoon, J.H., Ahn, J.H. and Lee, S.W. (2009), “Experimental study on behaviors of pile-abutment joint in integral abutment bridge”, *J. Kor. Soc. Civ. Eng*., **29**(6A), 651-659.

Kim, S.H., Yoon, J.H., Kim, J.H., Choi, W.J. and Ahn, J.H. (2012), “Structural details of steel girder-abutment joints in integral bridges: An experimental study”, *J. Construct. Steel Res*., **70**, 190-212.

Kim, W.S. and Laman, J.A. (2010), “Integral abutment bridge response under thermal loading”, *Eng. Struct*., **32**(6), 1495-1508.

Kim, W.S. and Laman, J.A. (2013), “Integral abutment bridge behavior under uncertain thermal and time-dependent load”, *Struct. Eng. Mech*., **46**(1), 53-73.

KRA (2012), *Bridge Design Specifications*, Korea Road Association, Seoul, Korea (in Korean).

LaFave, J.M., Riddle, J.K., Jarrett, M.W., Wright, B.A., Svatora, J.S., An, H. and Fahnestock, L.A. (2016), “Numerical simulations of steel integral abutment bridges under thermal loading”, *J. Bridge Eng*., **21**(10), 1-17.

Lemnitzer, A., Ahlberg, E.R., Nigbor, R.L., Shamsabadi, A., Wallace, J.W. and Stewart, J.P. (2009), “Lateral performance of full-scale bridge abutment wall with granular backfill”, *J. Geotech. Geoenviron. Eng*., **135**(4), 506-514.

MIDAS, I.T. (2012), *Midas Civil 2012 User Manual*, MIDAS Information Technology Co., Ltd. (in Koream).

MLTMA (2008), *Korea Bridge Design Code*, Ministry of Land, Transport and Maritime Affairs, Seoul, Korea (in Korean).

MLTMA (2012), *Korea Bridge Design Code (Limit State Design)*, Ministry of Land, Transport and Maritime Affairs, Seoul, Korea (in Korean).

Nam, M.S. and Park, Y.H. (2007), “Long-term behavior of Earth pressure on integral abutments”, *J. Kor. Geotech. Soc*., **23**(4), 47-58.

Nam, M.S., Do, J.N., Kim, T.S., Park, Y.H. and Kim, H.J. (2016), *Development of IPM Bridge*, Korea Expressway Corporation Research Institute, Hwaseong, Korea (in Korean).

Olson, S.M., Holloway, K.P., Buenker, J.M., Long, J.H. and LaFave, J.M. (2013), “Thermal behavior of IDOT integral abutment bridges and proposed design modifications”, FHWA-ICT-12-022, Illinois Center for Transportation, Rantoul, Illinois, U.S.A.

Olson, S.M., Long, J.H., Hansen, J.R., Renekis, D. and LaFave, J.M. (2009), “Modification of IDOT integral abutment design limitations and details”, FHWA-ICT-09-054, Illinois Center for Transportation, Rantoul, Illinois, U.S.A.

Park, Y.H. and Nam, M.S. (2007), “Behavior of earth pressure and movements on integral abutments”, *J. Kor. Soc. Civ. Eng*., **27**(3C), 163-173 (in Korean).

Reese, L., Wang, S., Isenhower, W. and Arrellaga, J. (2004), *LPILE Plus 5.0 for Windows*, Technical and User Manuals, ENSOFT Inc., Austin, Texas, U.S.A.

Reese, L.C. and Wang, S. (2006), *Verification of Computer Program LPile as a Valid Tool for Design of a Single Pile under Lateral Loading*, ENSOFT Inc., Austin, Texas, U.S.A., <www.ensoftinc.com>.

Reese, L.C., Cox, W.R. and Koop, F.D. (1974), *Analysis of Laterally Loaded Piles in Sand*, in *Offshore Technology in Civil Engineering Hall of Fame Papers from the Early Years*, OTC 2080, American Society of Civil Engineers, Reston, Virginia, U.S.A., 95-105.

Scott, R.F. (1981), *Foundation Analysis*, Prentice-Hall, Englewood, Cliffs, New Jersey, U.S.A.

VTrans (2008), *Integral Abutment Bridge Design Guidelines*, VTrans Integral Abutment Committee, State of Vermont, Agency of Transportation, Montpelier, Vermont, U.S.A., 1-92.

CC